AIAA JOURNAL
Vol. 43, No. 3, March 2005

Structural Behavior of Thin- and Thick-Walled Composite Blades with Multicell Sections

Sung Nam Jung* and Il Ju Park†
Chonbuk National University, Jeonju 561-756, Republic of Korea

A mixed beam approach that combines both the stiffness and the flexibility formulation in a unified manner has been performed to model and analyze coupled composite blades with closed, multiple-celled cross sections. The analysis model includes the effects of elastic couplings, shell wall thickness, transverse shear deformation, torsion warping, and constrained warping. Reissner's semicomplementary energy functional is used to derive the beam force–displacement relations. The influence of the shell bending strain measures as well as the membrane strain measures are incorporated in the formulation. For completeness required in a rigorous beam theory, four separate continuity conditions are imposed on each cell of the closed, multicelled sections. The theory is validated against experimental test data, detailed finite element analysis results, and other analytical results found in the literature for coupled composite beams and blades with various cross sections. These include two-cell box beams with bending–torsion and/or extension–torsion couplings and bending–torsion coupled composite blades with two-cell airfoils. The correlation between the present theory and other methods is found to be good, dependent on the geometries and material distributions adopted in the blades. Numerical results showing the effects of including the shell bending strain measures are examined. The effects of inappropriate treatment of the direction of integration for two-celled composite beams are also investigated in the current framework of the analysis.

Nomenclature

a	=	local shell radius of curvature
E_{11}, E_{22}	=	Young's moduli in principal directions
G_{12}	=	shear modulus
l	=	length of the blade
M_{xx}, M_{ss}, M_{xs}	=	moment resultants for the shell
M_y, M_z	=	beam bending moments
M_ω	=	warping moment
N	=	axial force of beam
N_{xn}, N_{sn}	=	transverse shear stress resultants for the shell
N_{xx}, N_{ss}, N_{xs}	=	membrane stress resultants for the shell segment
T	=	total torque, $T_s + T_\omega$
T_s	=	St. Venant torque
T_ω	=	Vlasov torque
U, V, W	=	beam displacements
u, v_t, v_n	=	shell displacements
V_y, V_z	=	transverse shear forces
x, s, n	=	coordinate systems for the shell wall
x, y, z	=	undeformed beam coordinates
β_y, β_z	=	section rotations for the beam
γ_{xy}, γ_{xz}	=	transverse shear strains for the beam
ε_{xx}, ε_{ss}, γ_{xs}	=	membrane strains for the shell
κ_{xx}, κ_{ss}, κ_{xs}	=	curvatures
ν_{12}	=	Poisson's ratio in principal plane
ϕ	=	elastic twist deformation
ψ_x, ψ_s	=	shell rotations

Subscripts

$,s$	=	partial derivative with s
$,x$	=	partial derivative with x

Superscript

T	=	transpose of a vector

Introduction

COMPOSITE rotor blades are, in general, builtup structures made of different materials for the skin and spar, normally of closed single- or multicelled cross-sections, and thin walled except near the root where they become thick walled. Common to both thin- and thick-walled blade analysis is the need to model properly the local behavior of the shell wall as a reaction to the global deformation of the blade. The wall undergoes both in-plane and out-of-plane warpings in response to the applied external loading. It is important to model these warpings correctly for the estimation of cross-sectional properties and eventually to get accurate analysis results for the beam response. At the present time, there is a good understanding of the significance of incorporating these warpings, and many advanced beam models have been developed in the relevant fields.[1,2] However, to date, highly reliable generic beam models for coupled composite blades, especially with multicelled sections, are extremely rare in the published literature.

There have been a few selected research activities to model and analyze composite beams and blades with multicell sections. Mansfield[3] developed a flexibility formulation for thin-walled composite beams with a two-cell cylindrical tube section. The equilibrium equations of the shell wall were used to derive the (4×4) flexibility matrix that captured the classical four beam variables (extension, bendings in two perpendicular planes, and torsion). The developed theory utilized only the membrane parts of the shell wall. Chandra and Chopra[4,5] investigated the structural response of thin-walled composite blades with two-cell sections analytically and experimentally. The stiffness matrix obtained by a displacement-based approach was of the order of (9×9), including the derivatives of shear strains. For constitutive relations, the in-plane strains and curvatures were assumed as zero in the shell wall. This assumption, which was similar to that of the classical plain-strain type, could actually lead to a stiffer response, especially in torsion for cases

Presented as Paper 2002-1432 at the 43rd Structures, Structural Dynamics, and Materials Conference, Denver, CO, 7–12 April 2002; received 16 August 2004; revision received 11 October 2004; accepted for publication 12 October 2004. Copyright © 2004 by the American Institute of Aeronautics and Astronautics, Inc. All rights reserved. Copies of this paper may be made for personal or internal use, on condition that the copier pay the $10.00 per-copy fee to the Copyright Clearance Center, Inc., 222 Rosewood Drive, Danvers, MA 01923; include the code 0001-1452/05 $10.00 in correspondence with the CCC.

*Associate Professor, Department of Aerospace Engineering. Senior Member AIAA.

†Graduate Research Assistant, Department of Aerospace Engineering.

with certain elastic couplings.[6] It is believed that this research has pioneered in providing the benchmark experimental results for the related fields.

Volovoi and Hodges[7] developed closed-form expressions for the stiffness matrices that contained the four classical beam variables by using the variational-asymptotic beam approach. For the asymptotic procedure, a few nondimensional parameters such as a/l or t/a, where a was the characteristic dimension of a cross section and t was the wall thickness, were introduced to eliminate small terms. They held that shell bending strain measures as well as constraint conditions for each cell of the section were not taken into account consistently in the published literature. Coupled composite beams with single- and double-celled box sections were considered to examine the effects of shell bending strain measures and hoop moments on the beam behavior. The results were correlated with their finite element analysis code VABS.

Jung et al.[8] developed a mixed beam theory that took into account the effects of the shell wall thickness, elastic couplings, transverse shear deformation, warping, warping restraint, and bending and shear of the shell wall. The term mixed was used because the direct stresses were treated as the known variables in terms of assumed displacements, whereas the shear flow and hoop moment in the shell wall were treated as the unknowns. The resulting (7×7) stiffness matrix characterized elastic properties of the beam in terms of the axial, flap and lag bending, flap and lag shear, torsion, and torsion–warping deformations. The theory was applied to open and closed (single-cell) cross section beams, and a good correlation was achieved in comparison with the experimental test data.

In the present work, the mixed formulation developed in Ref. 8 is extended to cover the multiple-celled section blades. Reissner's semicomplementary energy functional is used to derive the beam force–displacement relations. The formulation is validated by comparing the values of cross-sectional properties and steady responses of multicelled section beams and blades with experimental results and those from existing analysis methods found in the literature. In addition, a detailed finite element structural analysis using MSC/NASTRAN is carried out to correlate the current analysis. The effects of shell bending strain measures and inappropriate treatment of the direction of integration on the structural response of two-celled composite beams are also investigated.

As a matter of fact, the present theory shares a lot of common features with that of Volovoi and Hodges.[7] However, compared with the theory in Ref. 7, the present analysis has additional features in that 1) the influence of the thickness of the shell wall including the shear deformation (Reissner–Mindlin) effects are included, 2) warping restraint effects are included, and 3) no asymptotic arguments to delete any terms are employed in the current analysis.

Formulation

Figure 1 shows the geometry and coordinate systems of a composite blade with a two-cell cross section. Two systems of coordinate axes are used: an orthogonal Cartesian coordinate system (x, y, z) for the blade, where x is the reference axis of the blade and y and z are the transverse coordinates of the cross section, and a curvilinear coordinate system (x, s, n) for the shell wall of the section, where s is a contour coordinate measured along the middle surface of the shell wall and n is normal to this contour coordinate. The global deformations of the beam are U, V, and W along the x, y, and z axes, respectively, and ϕ is the elastic twist about the x axis. The local shell deformations are u, v_t, and v_n along the x, s, and n directions, respectively. When transverse shear deformations are allowed, the local deformations at an arbitrary point on the shell wall are expressed as

$$u = u^0 + n\psi_x, \qquad v_t = v_t^0 + n\psi_s, \qquad v_n = v_n^0 \tag{1}$$

In Eq. (1), u^0, v_t^0, and v_n^0 are the deformations at the midplane contour of the shell wall and ψ_x and ψ_s are rotations of the normal to the midplane about the s and x axes, respectively. From a geometric consideration, the shell midplane displacements can be expressed in terms of the beam displacements and rotations as

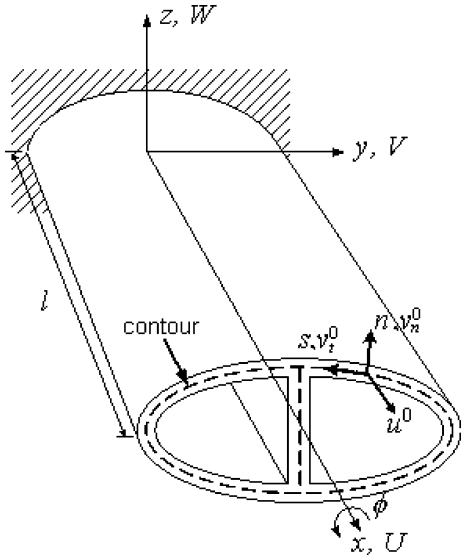

Fig. 1 Geometry and coordinate systems of a two-cell blade.

$$v_t^0 = Vy_{,s} + Wz_{,s} + r\phi, \qquad v_n^0 = Vz_{,s} - Wy_{,s} - q\phi$$
$$\psi_s = \phi \tag{2}$$

where r and q are the coordinates of an arbitrary point on the shell wall in the (n, s) coordinate system (Ref. 8) and the comma refers to the derivative with respect to the coordinate. The shell rotation ψ_x can be obtained by equating the shear strain γ_{xn} from the relation

$$\psi_x = v_{n,x}^0 - \gamma_{xn}, \qquad \gamma_{xn} = \gamma_{xy}z_{,s} - \gamma_{xz}y_{,s} \tag{3}$$

where γ_{xy} and γ_{xz} are the shear strains of the blade and are related to the cross section rotations β_y and β_z about the y and z axes, respectively,

$$\beta_y = \gamma_{xz} - W_{,x}, \qquad \beta_z = \gamma_{xy} - V_{,x} \tag{4}$$

When Eqs. (1–3) are used, the strain–displacement relation of the shell wall are obtained as

$$\varepsilon_{xx} = U_{,x} + z\beta_{y,x} + y\beta_{z,x} - \bar{\omega}\phi_{,xx}$$
$$\gamma_{xs} = \gamma_{xy}y_{,s} + \gamma_{xz}z_{,s} = u_{,s}^0 + V_{,x}y_{,s} + W_{,x}z_{,s} + r\phi_{,x}$$
$$\kappa_{xx} = \beta_{z,x}z_{,s} - \beta_{y,x}y_{,s} + q\phi_{,xx}$$
$$\kappa_{xs} = 2\phi_{,x} + (1/a)(\beta_z y_{,s} + \beta_y z_{,s} - r\phi_{,x}) \tag{5}$$

where $\bar{\omega}$ is the sectorial area of the cross section.[8] The strain–displacement relations of Eq. (5) form the basis of the displacement method for thin/thick-walled blades.

When the hoop stress flow N_{ss} is assumed to be negligibly small, the constitutive relations for the shell wall of the section can be written as

$$\begin{Bmatrix} N_{xx} \\ N_{xs} \\ M_{xx} \\ M_{ss} \\ M_{xs} \end{Bmatrix} = \begin{bmatrix} A'_{11} & A'_{16} & B'_{11} & B'_{12} & B'_{16} \\ A'_{16} & A'_{66} & B''_{16} & B'_{26} & B'_{66} \\ B'_{11} & B''_{16} & D'_{11} & D'_{12} & D'_{16} \\ B'_{12} & B'_{26} & D'_{12} & D'_{22} & D'_{26} \\ B'_{16} & B'_{66} & D'_{16} & D'_{26} & D'_{66} \end{bmatrix} \begin{Bmatrix} \varepsilon_{xx} \\ \gamma_{xs} \\ \kappa_{xx} \\ \kappa_{ss} \\ \kappa_{xs} \end{Bmatrix} \tag{6}$$

where

$$A'_{11} = A_{11} - A_{12}^2/A_{22}, \qquad A'_{16} = A_{16} - A_{12}A_{26}/A_{22}$$

$$A'_{66} = A_{66} - A_{26}^2/A_{22}, \qquad B'_{11} = B_{11} - A_{12}B_{12}/A_{22}$$

$$B'_{12} = B_{12} - A_{12}B_{22}/A_{22}, \qquad B'_{16} = B_{16} - A_{12}B_{26}/A_{22}$$

$$B''_{16} = B_{16} - A_{26}B_{12}/A_{22}, \qquad B'_{26} = B_{26} - A_{26}B_{22}/A_{22}$$

$$B'_{66} = B_{66} - A_{26}B_{26}/A_{22}, \qquad D'_{11} = D_{11} - B_{12}^2/A_{22}$$

$$D'_{12} = D_{12} - B_{12}B_{22}/A_{22}, \qquad D'_{16} = D_{16} - B_{12}B_{26}/A_{22}$$

$$D'_{22} = D_{22} - B_{22}^2/A_{22}, \qquad D'_{26} = D_{26} - B_{22}B_{26}/A_{22}$$

$$D'_{66} = D_{66} - B_{26}^2/A_{22} \tag{7}$$

where A_{ij}, B_{ij}, and D_{ij} are the laminate stiffnesses for extension, entension–bending coupling, and bending, respectively.[9] In the present approach, we treat the strain measures ε_{xx}, κ_{xx}, and κ_{xs} as the known and derive expressions for the shear flow N_{xs} and the hoop moment M_{ss} in terms of the known quantities by using the equilibrium equations of the shell wall. It is convenient to write Eq. (6) in a semi-inverted form as

$$\begin{Bmatrix} N_{xx} \\ M_{xx} \\ M_{xs} \\ \gamma_{xs} \\ \kappa_{ss} \end{Bmatrix} = \begin{bmatrix} C_{n\varepsilon} & C_{n\kappa} & C_{n\phi} & C_{n\gamma} & C_{n\tau} \\ C_{n\kappa} & C_{m\kappa} & C_{m\phi} & C_{m\gamma} & C_{m\tau} \\ C_{n\phi} & C_{m\phi} & C_{\phi\phi} & C_{\phi\gamma} & C_{\phi\tau} \\ -C_{n\gamma} & -C_{m\gamma} & -C_{\phi\gamma} & C_{\gamma\gamma} & C_{\gamma\tau} \\ -C_{n\tau} & -C_{m\tau} & -C_{\phi\tau} & C_{\gamma\tau} & C_{\tau\tau} \end{bmatrix} \begin{Bmatrix} \varepsilon_{xx} \\ \kappa_{xx} \\ \kappa_{xs} \\ N_{xs} \\ M_{ss} \end{Bmatrix} \tag{8}$$

To assess the semi-inverted constitutive relations (8) into the beam formulation, a modified form of the Reissner's semicomplementary energy functional Φ_R is introduced,

$$\Phi_R = \tfrac{1}{2}[N_{xx}\varepsilon_{xx} + M_{xx}\kappa_{xx} + M_{xs}\kappa_{xs} - N_{xs}\gamma_{xs} - M_{ss}\kappa_{ss}] \tag{9}$$

The stiffness matrix relating beam forces to displacements is obtained by using the variational statement of the Reissner functional, which is given by

$$\delta \int_0^l \oint (\Phi_R + \gamma_{xs}N_{xs} + \kappa_{ss}M_{ss})\,\mathrm{d}s\,\mathrm{d}x = 0 \tag{10}$$

Performing the x integrals, Eq. (10) results in the equilibrium equations of an element of the shell wall

$$N_{xx,x} + N_{xs,s} = 0, \qquad N_{xs,x} = 0$$

$$M_{xx,x} + M_{xs,s} = 0, \qquad M_{xs,x} + M_{ss,s} = 0 \tag{11}$$

as well as the constraint conditions

$$\gamma_{xs} - u^0_{,s} - v^0_{t,x} = 0, \qquad \kappa_{ss} - \psi_{s,s} = 0 \tag{12}$$

Performing the s-integrals in the first two equations of Eq. (11) indicates that N_{xs} consists of a constant part and a part that depends on the s integral of $N_{xx,x}$. In addition, it is found from the third and fourth equations in Eq. (11) that M_{ss} has a constant part, a part that varies linearly with s, and a part that depends on the s integral of $M_{xs,x}$. Hence, one can write the expression for the shear flow N_{xs} and the hoop moment M_{ss} as

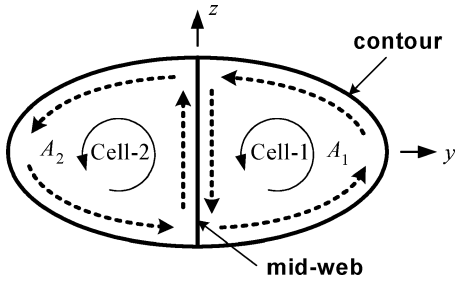

Fig. 2 Definition of a two-cell section.

$$N_{xs} = N^0_{xs} - \int_0^s N_{xx,x}\,\mathrm{d}s$$

$$M_{ss} = M^0_{ss} + yM^y_{ss} + zM^z_{ss} - \int_0^s M_{xs,x}\,\mathrm{d}s \tag{13}$$

where N^0_{xs}, M^0_{ss}, M^y_{ss}, and M^z_{ss} represent the circuit shear flows and hoop moments for each cell of a closed multicell section. For a two-cell blade, these lead to eight unknowns that are expressed as

$$\{n\} = \left\lfloor \left(N^0_{xs}\right)_1 \quad \left(N^0_{xs}\right)_2 \quad \left(M^0_{ss}\right)_1 \quad \left(M^0_{ss}\right)_2 \quad \left(M^y_{ss}\right)_1 \quad \left(M^y_{ss}\right)_2 \quad \left(M^z_{ss}\right)_1 \quad \left(M^z_{ss}\right)_2 \right\rfloor^T \tag{14}$$

where the subscripts 1 and 2 refer to the first and the second cell, respectively (Fig. 2). The continuity conditions that must be satisfied for each cell of the two-celled section yield the following sets of equations:

$$\oint_1 \gamma_{xs}\,\mathrm{d}s = 2A_1\phi_{,x}, \qquad \oint_1 \kappa_{ss}\,\mathrm{d}s = 0, \qquad \oint_1 y\kappa_{ss}\,\mathrm{d}s = 0$$

$$\oint_1 z\kappa_{ss}\,\mathrm{d}s = 0, \qquad \oint_2 \gamma_{xs}\,\mathrm{d}s = 2A_2\phi_{,x}, \qquad \oint_2 \kappa_{ss}\,\mathrm{d}s = 0$$

$$\oint_2 y\kappa_{ss}\,\mathrm{d}s = 0, \qquad \oint_2 z\kappa_{ss}\,\mathrm{d}s = 0 \tag{15}$$

When the constitutive relations of Eq. (8) are substituted into Eq. (15), the unknown shear flows and hoop moments can be obtained as

$$\{n\} = [Q]^{-1} \cdot ([P]\{\bar{q}_b\} + \underline{[R]\{\bar{q}_{b,x}\}}) = [b]\{\bar{q}_b\} + \underline{[B]\{\bar{q}_{b,x}\}} \tag{16}$$

where the derivatives of the beam deformations $\{\bar{q}_b\}$ are defined as

$$\{\bar{q}_b\} = \left\lfloor U_{,x} \quad \beta_{y,x} \quad \beta_{z,x} \quad \phi_{,x} \quad \phi_{,xx} \right\rfloor^T \tag{17}$$

The underlined terms in Eq. (16) need not be evaluated because this will be determined in terms of the applied shear forces. The section integrals $[Q]$ and $[P]$ in Eq. (16) are a symmetric (8×8) matrix and a (8×5) matrix, respectively, for two-cell sections. They are expressed as

$$[Q] = \begin{bmatrix}
\oint_1 C_{\gamma\gamma}\,ds & -\int_w C_{\gamma\gamma}\,ds & \oint_1 C_{\gamma\tau}\,ds & -\int_w C_{\gamma\tau}\,ds & \oint_1 yC_{\gamma\tau}\,ds & -\int_w yC_{\gamma\tau}\,ds & \oint_1 zC_{\gamma\tau}\,ds & -\int_w zC_{\gamma\tau}\,ds \\
-\int_w C_{\gamma\gamma}\,ds & \oint_2 C_{\gamma\gamma}\,ds & -\int_W C_{\gamma\tau}\,ds & \oint_2 C_{\gamma\tau}\,ds & -\int_w yC_{\gamma\tau}\,ds & \oint_2 yC_{\gamma\tau}\,ds & -\int_w zC_{\gamma\tau}\,ds & \oint_2 zC_{\gamma\tau}\,ds \\
\oint_1 C_{\gamma\tau}\,ds & -\int_w C_{\gamma\tau}\,ds & \oint_1 C_{\tau\tau}\,ds & -\int_w C_{\tau\tau}\,ds & \oint_1 yC_{\tau\tau}\,ds & -\int_w yC_{\tau\tau}\,ds & \oint_1 zC_{\tau\tau}\,ds & -\int_w zC_{\tau\tau}\,ds \\
-\int_w C_{\gamma\tau}\,ds & \oint_2 C_{\gamma\tau}\,ds & -\int_W C_{\tau\tau}\,ds & \oint_2 C_{\tau\tau}\,ds & -\int_w yC_{\tau\tau}\,ds & \oint_2 yC_{\tau\tau}\,ds & -\int_w zC_{\tau\tau}\,ds & \oint_2 zC_{\tau\tau}\,ds \\
\oint_1 yC_{\gamma\tau}\,ds & -\int_w yC_{\gamma\tau}\,ds & \oint_1 yC_{\tau\tau}\,ds & -\int_w yC_{\tau\tau}\,ds & \oint_1 y^2C_{\tau\tau}\,ds & -\int_w y^2C_{\tau\tau}\,ds & \oint_1 yzC_{\tau\tau}\,ds & -\int_w yzC_{\tau\tau}\,ds \\
-\int_w yC_{\gamma\tau}\,ds & \oint_2 yC_{\gamma\tau}\,ds & -\int_W yC_{\tau\tau}\,ds & \oint_2 yC_{\tau\tau}\,ds & -\int_w y^2C_{\tau\tau}\,ds & \oint_2 y^2C_{\tau\tau}\,ds & -\int_w yzC_{\tau\tau}\,ds & \oint_2 yzC_{\tau\tau}\,ds \\
\oint_1 zC_{\gamma\tau}\,ds & -\int_w zC_{\gamma\tau}\,ds & \oint_1 zC_{\tau\tau}\,ds & -\int_w zC_{\tau\tau}\,ds & \oint_1 yzC_{\tau\tau}\,ds & -\int_w yzC_{\tau\tau}\,ds & \oint_1 z^2C_{\tau\tau}\,ds & -\int_w z^2C_{\tau\tau}\,ds \\
-\int_W zC_{\gamma\tau}\,ds & \oint_2 zC_{\gamma\tau}\,ds & -\int_W zC_{\tau\tau}\,ds & \oint_2 zC_{\tau\tau}\,ds & -\int_w yzC_{\tau\tau}\,ds & \oint_2 yzC_{\tau\tau}\,ds & -\int_w z^2C_{\tau\tau}\,ds & \oint_2 z^2C_{\tau\tau}\,ds
\end{bmatrix} \tag{18}$$

$$[P] = \begin{bmatrix}
\oint_1 C_{n\gamma}\,ds & \oint_1 (zC_{n\gamma} - y_{,s}C_{m\gamma})\,ds & \oint_1 (yC_{n\gamma} + z_{,s}C_{m\gamma})\,ds & 2A_1 + 2\oint_1 C_{\phi\gamma}\,ds & \oint_1 (-\bar{\omega}C_{n\gamma} + qC_{m\gamma})\,ds \\
\oint_2 C_{n\gamma}\,ds & \oint_2 (zC_{n\gamma} - y_{,s}C_{m\gamma})\,ds & \oint_2 (yC_{n\gamma} + z_{,s}C_{m\gamma})\,ds & 2A_2 + 2\oint_2 C_{\phi\gamma}\,ds & \oint_2 (-\bar{\omega}C_{n\gamma} + qC_{m\gamma})\,ds \\
\oint_1 C_{n\tau}\,ds & \oint_1 (zC_{n\tau} - y_{,s}C_{m\tau})\,ds & \oint_1 (yC_{n\tau} + z_{,s}C_{m\tau})\,ds & 2\oint_1 C_{\phi\tau}\,ds & \oint_1 (-\bar{\omega}C_{n\tau} + qC_{m\tau})\,ds \\
\oint_2 C_{n\tau}\,ds & \oint_2 (zC_{n\tau} - y_{,s}C_{m\tau})\,ds & \oint_2 (yC_{n\tau} + z_{,s}C_{m\tau})\,ds & 2\oint_2 C_{\phi\tau}\,ds & \oint_2 (-\bar{\omega}C_{n\tau} + qC_{m\tau})\,ds \\
\oint_1 yC_{n\tau}\,ds & \oint_1 (yzC_{n\tau} - yy_{,s}C_{m\tau})\,ds & \oint_1 \left(y^2C_{n\tau} + yz_{,s}C_{m\tau}\right)ds & 2\oint_1 yC_{\phi\tau}\,ds & \oint_1 (-y\bar{\omega}C_{n\tau} + yqC_{m\tau})\,ds \\
\oint_2 yC_{n\tau}\,ds & \oint_2 (yzC_{n\tau} - yy_{,s}C_{m\tau})\,ds & \oint_2 \left(y^2C_{n\tau} + yz_{,s}C_{m\tau}\right)ds & 2\int_2 yC_{\phi\tau}\,ds & \oint_2 (-y\bar{\omega}C_{n\tau} + yqC_{m\tau})\,ds \\
\oint_1 zC_{n\tau}\,ds & \oint_1 \left(z^2C_{n\tau} - zy_{,s}C_{m\tau}\right)ds & \oint_1 (yzC_{n\tau} + zz_{,s}C_{m\tau})\,ds & 2\oint_1 zC_{\phi\tau}\,ds & \oint_1 (-z\bar{\omega}C_{n\tau} + zqC_{m\tau})\,ds \\
\oint_2 zC_{n\tau}\,ds & \oint_2 \left(z^2C_{n\tau} - zy_{,s}C_{m\tau}\right)ds & \oint_2 (yzC_{n\tau} + zz_{,s}C_{m\tau})\,ds & 2\oint_2 zC_{\phi\tau}\,ds & \oint_2 (-z\bar{\omega}C_{n\tau} + zqC_{m\tau})\,ds
\end{bmatrix} \tag{19}$$

where A_1 and A_2 are the areas of each cell and the subscript w designated in Eq. (18) refers to the midplane web of the two-cell section (Fig. 2). For a m-celled section, the $[Q]$ and $[P]$ result in $(4m \times 4m)$ and $(4m \times 5)$ matrices, respectively. Note that the direction of integration for each cell should be chosen carefully because a common boundary exists between the two cells when the direction of integration is taken as in Fig. 2. In this case, the middle member must be integrated in the opposite direction for the right and left cell, respectively.

When Eqs. (15) and (16) are combined, the expression for the shear flow and the hoop moment can be obtained as

$$\begin{Bmatrix} N_{xs} \\ M_{ss} \end{Bmatrix}_{\text{cell-1}} = \begin{bmatrix} f_{x1} & f_{y1} & f_{z1} & f_{\phi 1} & f_{\omega 1} \\ g_{x1} & g_{y1} & g_{z1} & g_{\phi 1} & g_{\omega 1} \end{bmatrix} \{\bar{q}_b\} + \begin{Bmatrix} N^r_{xs} \\ M^r_{ss} \end{Bmatrix}_1 \tag{20a}$$

$$\begin{Bmatrix} N_{xs} \\ M_{ss} \end{Bmatrix}_{\text{cell-2}} = \begin{bmatrix} f_{x2} & f_{y2} & f_{z2} & f_{\phi 2} & f_{\omega 2} \\ g_{x2} & g_{y2} & g_{z2} & g_{\phi 2} & g_{\omega 2} \end{bmatrix} \{\bar{q}_b\} + \begin{Bmatrix} N^r_{xs} \\ M^r_{ss} \end{Bmatrix}_2 \tag{20b}$$

where

$$\begin{Bmatrix} f_{x1} \\ f_{y1} \\ f_{z1} \\ f_{\phi 1} \\ f_{\omega 1} \end{Bmatrix} = \begin{Bmatrix} b_{11} \\ b_{12} \\ b_{13} \\ b_{14} \\ b_{15} \end{Bmatrix}, \qquad \begin{Bmatrix} g_{x1} \\ g_{y1} \\ g_{z1} \\ g_{\phi 1} \\ g_{\omega 1} \end{Bmatrix} = \begin{Bmatrix} b_{31} + yb_{51} + zb_{71} \\ b_{32} + yb_{52} + zb_{72} \\ b_{33} + yb_{53} + zb_{73} \\ b_{34} + yb_{54} + zb_{74} \\ b_{35} + yb_{55} + zb_{75} \end{Bmatrix} \tag{21a}$$

$$\begin{Bmatrix} f_{x2} \\ f_{y2} \\ f_{z2} \\ f_{\phi 2} \\ f_{\omega 2} \end{Bmatrix} = \begin{Bmatrix} b_{21} \\ b_{22} \\ b_{23} \\ b_{24} \\ b_{25} \end{Bmatrix}, \qquad \begin{Bmatrix} g_{x2} \\ g_{y2} \\ g_{z2} \\ g_{\phi 2} \\ g_{\omega 2} \end{Bmatrix} = \begin{Bmatrix} b_{41} + yb_{61} + zb_{81} \\ b_{42} + yb_{62} + zb_{82} \\ b_{43} + yb_{63} + zb_{83} \\ b_{44} + yb_{64} + zb_{84} \\ b_{45} + yb_{65} + zb_{85} \end{Bmatrix} \tag{21b}$$

where b_{ij} is the corresponding component of the ith row and jth column of matrix $[b]$, which is defined in Eq. (16). Volovoi and Hodges[7] obtained similar expressions for the shear flows and hoop moments. Based on an asymptotic argument, they discard $\phi_{,xx}$ for closed-section beams and also the terms corresponding to the derivatives

of $\bar{q}_b$. In Eq. (20), the first part of the shear flows and hoop moments that is dependent on the strain measures can be thought to be the active part of the shear flow, whereas the second part is dependent on the applied forces and can be thought to be the reactive shear flow according to the terminology used by Gjelsvik.[10] The superscript r in Eq. (20) reflects this aspect.

In the present method, all of the terms are retained in Eq. (20), and Eq. (10) is used to identify the cross section stress resultants as

$$N = \oint N_{xx}\,\mathrm{d}s, \qquad M_y = \oint [N_{xx}z - M_{xx}y_{,s}]\,\mathrm{d}s$$

$$M_z = \oint [N_{xx}y + M_{xx}z_{,s}]\,\mathrm{d}s, \qquad M_\omega = \oint [-N_{xx}\bar{\omega} + M_{xx}q]\,\mathrm{d}s$$

$$T_s = \oint [2M_{xs}]\,\mathrm{d}s \tag{22a}$$

$$V_y = \oint N_{xs}y_{,s}\,\mathrm{d}s, \qquad V_z = \oint N_{xs}z_{,s}\,\mathrm{d}s \tag{22b}$$

where M_y and M_z are bending moments about y and z directions, respectively, T_s is St. Venant twisting moment, and M_ω is Vlasov bimoment. When Eqs. (5) and (8) are substituted into Eq. (22a), the following relations can be obtained:

$$\{\bar{F}_b\} = \lfloor N \quad M_y \quad M_z \quad T \quad M_\omega \rfloor^T = [C]\{\bar{q}_b\} + [D]\{\bar{q}_{b,x}\} \tag{23}$$

where $[C]$ is a symmetric (5×5) cross section stiffness matrix that represents the idealization of the beam at an Euler–Bernoulli level for extension and bending and Vlasov for torison. The elements of the matrix $[D]$ are functions of the shear flow, the hoop moment, and also the derivatives of the strain measures.

To obtain the equivalent of a Timoshenko (first-order shear deformation) theory for the blade, we consider a cantilever blade with shear forces V_y and V_z applied at the tip. Differentiating Eq. (23) with respect to x, we obtain

$$\{\bar{F}_{b,x}\} = \{F_s\} = \lfloor 0 \quad V_z \quad V_y \quad 0 \quad 0 \rfloor^T = [C]\{\bar{q}_{b,x}\} \tag{24}$$

or

$$\{\bar{q}_{b,x}\} = [C]^{-1}\{F_s\} \tag{25}$$

From Eq. (22b), one can obtain the force vector $\{F_s\}$ as

$$\{F_s\} = [E]\{q\} \tag{26}$$

where $\{q\}$ is the generalized displacement vector defined as

$$\{q\} = \lfloor U_{,x} \quad \beta_{y,x} \quad \beta_{z,x} \quad \phi_{,x} \quad \phi_{,xx} \quad \gamma_{xy} \quad \gamma_{xz} \rfloor^T \tag{27}$$

From Eqs. (23), (25), and (26), the following equations relating beam forces and displacements are obtained:

$$\{F\} = [K]\{q\} \tag{28}$$

where the generalized force vector $\{F\}$ is given by

$$\{F\} = \lfloor N \quad M_y \quad M_z \quad T \quad M_\omega \quad V_y \quad V_z \rfloor^T \tag{29}$$

The stiffness matrix $[K]$ in Eq. (28) has an order of (7×7), represents the beam stiffness matrix at a Timoshenko level for bending and shear and a Vlasov level for torsion, and includes the influence of the shell wall thickness.

Results and Discussion

A numerical investigation has been performed to correlate the current analysis with available literature and also with detailed finite element analysis results. The examples include two-cell composite box beams with extension–torsion and/or bending–torsion couplings and bending–torsion coupled composite blades with a two-cell airfoil section. For the present results to be described in this section, the effects of transverse shear couplings are not included in the analysis because the transverse shear couplings have a marginal effect for beams with high slenderness ratios. Note that the slenderness ratio is defined as the ratio of effective length to height of the beam. The corresponding slenderness ratios are larger than 60 for the cases considered in this study. In this case, the error due to the neglect of the transverse shear is less than 1% for closed-section beams.[8]

Two-Cell Composite Box Beams

The first example is a two-celled composite box beam with extension–torsion couplings. Figure 3 is a schematic of the layup (box 1) used in the study. For this case, the top and bottom walls of the box section are composed of $[\theta_3/-\theta_3]$ layup, whereas all three vertical walls including the midweb are composed of $[-\theta_3/\theta_3]$ so that the extension–torsion couplings arise in the beam. As shown in Fig. 3, the normal to each wall is directed outward, and the stacking sequence is from top to bottom as is given in Ref. 9. The positive fiber orientation angle is defined as having right angles with respect to the outward normal vector in the walls. The geometry and material properties of composite box beams made of graphite–epoxy lamina are summarized in Table 1. This two-cell box configuration (box 1) has been studied by Volovoi and Hodges[7] to validate their theory and also to verify that most published results do not take into account consistently the bending shell strain measures as well as the constitutive relations.

Figure 4 shows the comparison of torsion rigidities for two-celled composite box beams having box 1 configuration as a function of ply orientation angles. In Fig. 4, the present results are compared with the analytical results predicted by Volovoi and Hodges[7] and with those of two-dimensional MSC/NASTRAN analysis. A variational-asymptotic beam approach is adopted for the results of Volovoi and Hodges. For the NASTRAN analysis, a finite element mesh composed of 6600 (150 along the beam span, 44 through the cross section) CQUAD4 elements is used to obtain the results. As can be seen in Fig. 4, there is a clear correlation between the results obtained by three different methods. The maximum error is less than 1%

Table 1 Geometry and material properties of two-cell composite box beams

Property	Value
E_{11}	141.9 GPa (20.59×10^6 psi)
E_{22}	9.78 GPa (1.42×10^6 psi)
G_{12}	6.13 GPa (0.89×10^6 psi)
ν_{12}	0.42
ρ	1449 kg/m^3 (0.05224 lb/in.^{3})
Ply thickness t_p	0.127 mm (0.005 in.)
Outer width $2b$	24.21 mm (0.953 in.)
Outer height $2h$	13.64 mm (0.537 in.)
Length l	762 mm (30 in.)

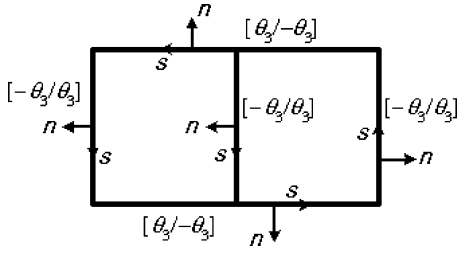

Fig. 3 Schematic of box 1 layup.

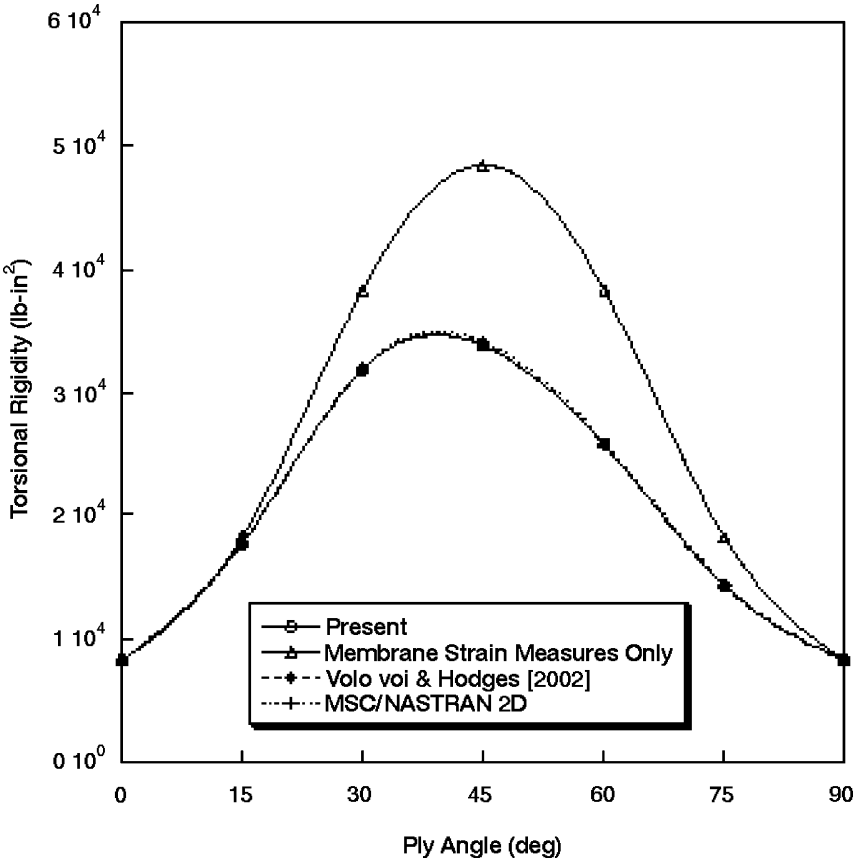

Fig. 4 Comparison of torsion rigidities for box 1 case with ply angle changes.

between three results. In Fig. 4, the present results with the bending strain measures neglected, which are designated as membrane strain measures only, are also included to identify the effects of the shell wall thickness separately. It is indicated that the theory without the bending strain measures included results in serious error for predicting the torsion stiffness. The error becomes 43.2% at 45 deg of ply angles. This kind of error is unavoidable when the analysis where the membrane formulation is used because the extension–twisting and bending–shearing couplings (B_{16} and B_{26}) are not taken into account in that formulation. Note that, for the $[\theta_3/-\theta_3]$ or $[-\theta_3/\theta_3]$ layup, the extension–shear (A_{16} and A_{26}) and bending–twisting (D_{16} and D_{26}) couplings become zero, whereas the extension–twisting and bending–shearing couplings (B_{16} and B_{26}) have nonzero values due to the antisymmetry of the layup against the midplane of the section.

Figure 5 shows the variation of flapwise bending rigidities as a function of fiber angles for the box 1 beam. The present results are compared with the MSC/NASTRAN two-dimensional results. The correlation is seen to be very good for this box 1 case. The influence of elastic couplings can be quite dramatic on the beam behavior. About a 1450% increase in bending rigidities is achieved by simply varying the fiber angles from 90 to 0 deg in the box-beam walls. Designers may exploit this additional influence by tailoring the structural properties in their specific applications for a greater performance.

Two other different box-beam cases are also considered to identify the effects of bending strain measures and also to confirm that the direction of integration has been treated consistently in the present analysis. Figure 6 shows the schematic of the two layup cases used in the study: The first one, designated as box 2, is a circumferentially uniform stiffness layup that leads to an extension–bending–torsion coupling. The second one (box 3) presents circumferentially asymmetric stiffness values along the contours that actually lead to a bending–torsion coupling. For both the box 2 and box 3 layups, the extension–shearing (A_{16} and A_{26}) and bending–twisting (D_{16} and D_{26}) couplings have nonzero values, whereas the extension–twisting and bending–shearing couplings (B_{16} and B_{26}) become zero.

Figure 7 shows the variation of torsional rigidities for box 2 beam as a function of ply orientation angles. The present results with and without the effects of bending strain measures are compared with those of the MSC/NASTRAN two-dimensional analysis. As expected, the effects of including the bending strain measures are not so critical compared to the earlier box 1 case because the important shell wall stiffnesses affecting the torsion property for the box 2 case are the extension–shearing (A_{16} and A_{26}) couplings. The maximum error induced by neglecting the bending strain measures is 1.2% at ply angles of 45 deg. The role of D_{16} and D_{26} in the complete formulation is the primary source of the difference between the two results. The correlation of the present results with the MSC/NASTRAN results is seen to be very good. In Fig. 7, the effects of inappropriate treatment of the direction of integration along the midweb for the two-cell box section are also presented. As mentioned in the Formulation section, the middle member must be integrated in the opposite direction for the right and left cell, respectively, due to the existence of a common boundary between the two cells as described in Fig. 2. Once the direction of the contour is changed, the outward normal vector should be changed accordingly, and this influences the sign (positive or negative) of the shell wall stiffness. The rectangles shown in Fig. 7 are the results obtained with the unilateral direction of the contour integration, whereas the other symbols indicate results obtained with the correct directions in the right and left cells, respectively. The maximum error induced by the inconsistent direction of integration is 29.5% at ply angles of 30 deg. Note that this kind of error may also be avoided by a careful selection of the direction of the integration throughout the contour, as suggested in Ref. 7.

The bending–torsion-coupled box 3 case is presented in Fig. 8. The maximum error due to the neglect of the bending strain measures for the box 3 case amounts to 4.6% at ply angles of 30 deg, which is slightly larger than that with the box 2 case. However, the error

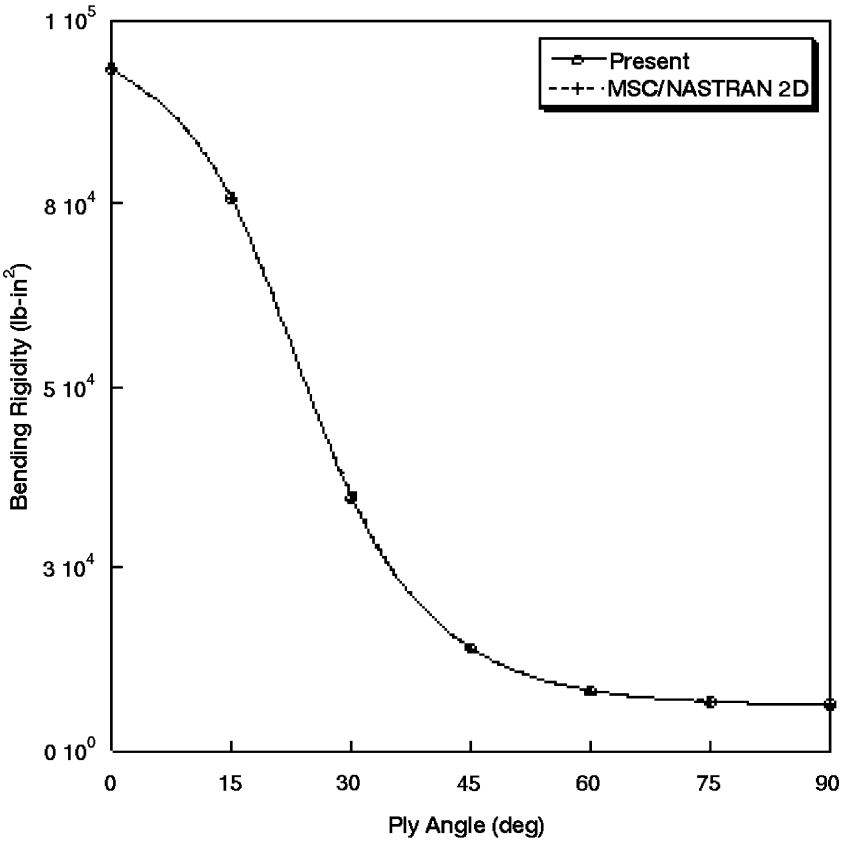

Fig. 5 Comparison of bending rigidities of box 1 case with ply angle changes.

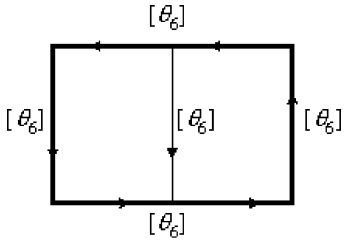

a) Layup of box 2

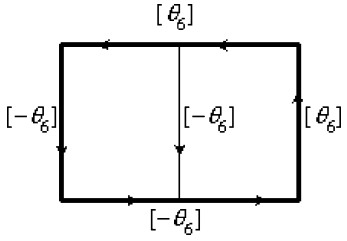

b) Layup of box 3

Fig. 6 Layup cases of boxes 2 and 3.

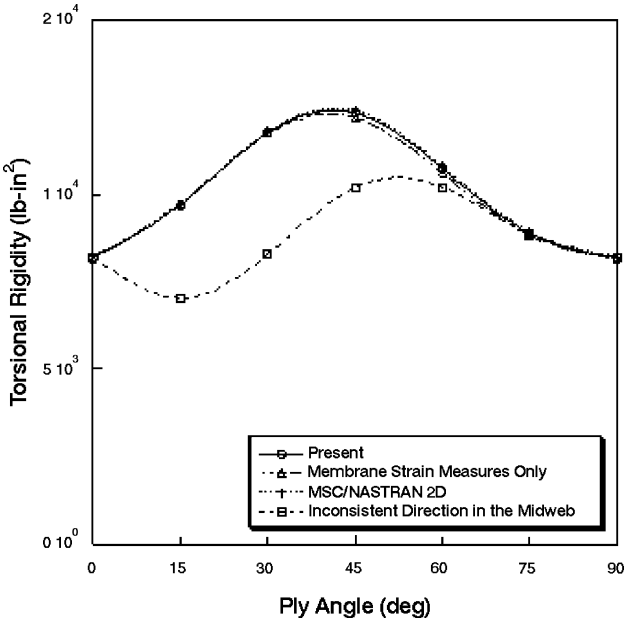

Fig. 7 Comparison of torsion rigidities for box 2 case with ply angle changes.

induced by the inconsistent direction of the integration becomes much smaller (maximum 5.5%) than that with the box 2 case. This is because the box 2 case has the bending–torsion couplings induced by the symmetry of the midweb laminates along with the extension–torsion couplings that finally leads to unconventional extension–bending–torsion couplings, whereas the box 3 case exhibits only the bending–torsion coupling.

Overall, the present predictions for coupled composite box beams with two-cell sections are in excellent agreements with those of the MSC/NASTRAN two-dimensional results and also with the available literature. Based on the correlation study, it is believed that the present theory can capture effectively both the classical and nonclassical structural effects of multiple-celled composite beams with a high accuracy.

Two-Cell Composite Blades

Next, a numerical study is carried out for elastically coupled composite blades with a two-cell airfoil section. Figure 9 shows the schematic of the two-cell blade section. The blade was originally studied in the work of Chandra and Chopra.[4,5] The section has a

Table 2 Geometry and material properties of two-cell composite blades

Property	Value
E_{11}	131 GPa (19×10^6 psi)
E_{22}	9.3 GPa (1.35×10^6 psi)
G_{12}	5.86 GPa (0.85×10^6 psi)
ν_{12}	0.40
Ply thickness	0.127 mm (0.005 in.)
Airfoil	NACA 0012
Length	641.4 mm (25.25 in.)
Chord	76.2 mm (3 in.)
Airfoil thickness	9.144 mm (0.36 in.)

Table 3 Layup cases of bending–torsion coupled composite blades

	Spar			
Case	Top flange	Bottom flange	Web	Skin
Blade 1	$[0/15]_4$	$[0/-15]_4$	$[0/\pm 15/0]_2$	[15/−15]
Blade 2	$[0/30]_4$	$[0/-30]_4$	$[0/\pm 30/0]_2$	[30/−30]
Blade 3	$[0/45]_4$	$[0/-45]_4$	$[0/\pm 45/0]_2$	[45/−45]

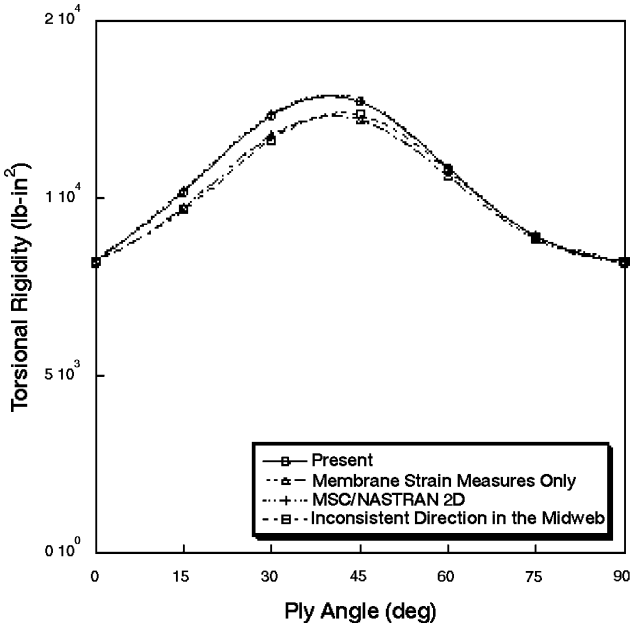

Fig. 8 Comparison of torsion rigidities for box 3 case with ply angle changes.

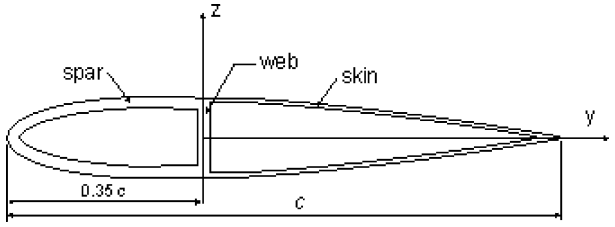

Fig. 9 Schematic of a two-cell blade section.

NACA 0012 contour and is composed of D-type spar and skin. The blade is clamped at one end, and warping is restrained at both ends. The geometry and the material properties of the blade are summarized in Table 2. Blades with three different ply layups representing bending–torsion couplings are examined. Table 3 shows the details of the layup used in this study.

Figure 10 shows the comparison results for both the tip bending slope and the induced tip twist of the bending–torsion coupled blade (blade 1) subjected to a unit tip bending load. As

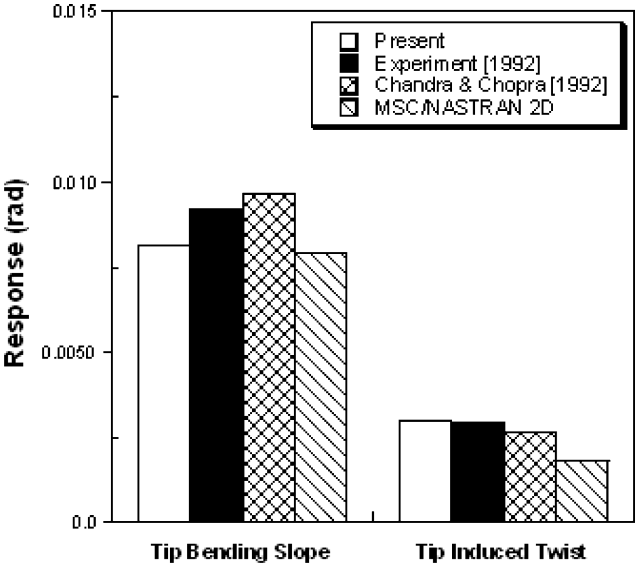

Fig. 10 Comparison of responses for two-cell composite blades (blade 1) under unit tip bending load.

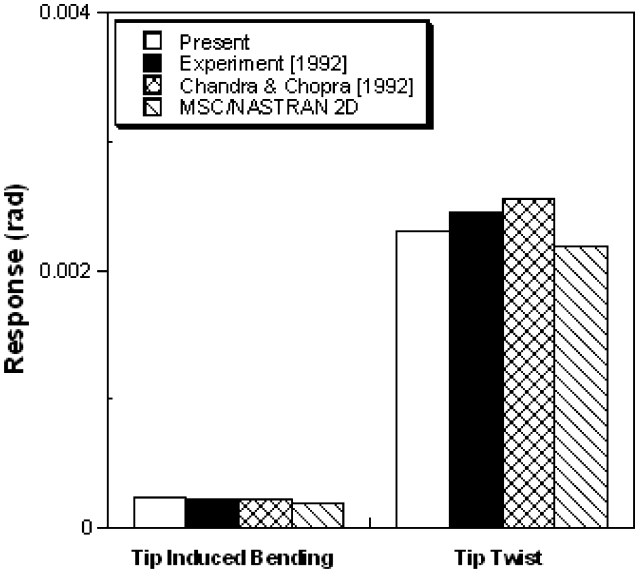

Fig. 11 Comparison of responses for two-cell composite blades (blade 1) under unit tip torque load.

given in Table 3, blade 1 consists of 15 deg ($[0/15]_4$) spar and ±15 deg ([15/−15]) skin. The present predictions are compared with the experimental test data and the theoretical results obtained by Chandra and Chopra[4,5] along with those of the two-dimensional MSC/NASTRAN analysis. For the NASTRAN results, a total of 15,800 CQUAD4 plate/shell finite elements totaling 77,721 degrees of freedom are used. For the present results, the contours in the rear and front parts of the NACA 0012 section are divided into 100 and 800 segments, respectively, to perform the numerical integration along the contour of the section. As can be seen in Fig. 10, the predictions obtained by the present method are in fair-to-good agreement with the other results for both the direct bending response and the induced response of the beam. The error between the present results and the experimental test data is 11.6% for the tip bending slopes and 1.7% for the induced twist response, respectively. The difference between the current predictions and the theoretical results of Ref. 6 is due mainly to that in Ref. 6 the zero-in-plane strain assumption ($\gamma_{ss} = \kappa_{ss} = 0$) is used for the constitutive relations, whereas, in the present approach, the zero hoop stress flow assumption ($N_{ss} = 0$) is used. In comparison with the NASTRAN

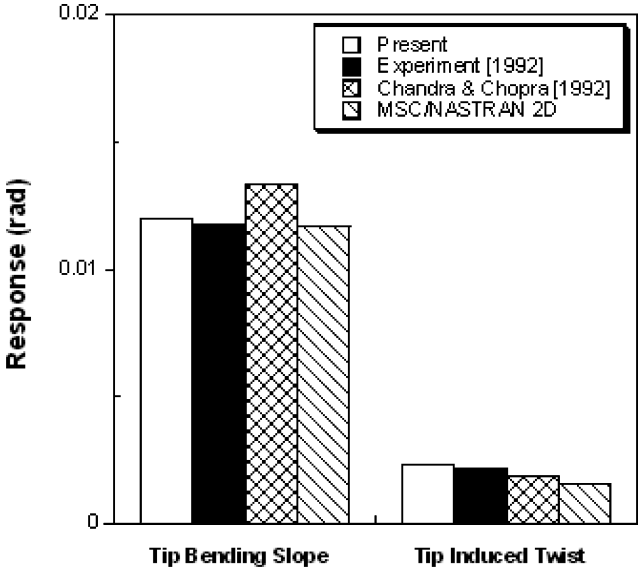

Fig. 12 Comparison of responses for two-cell composite blades (blade 2) under unit tip bending load.

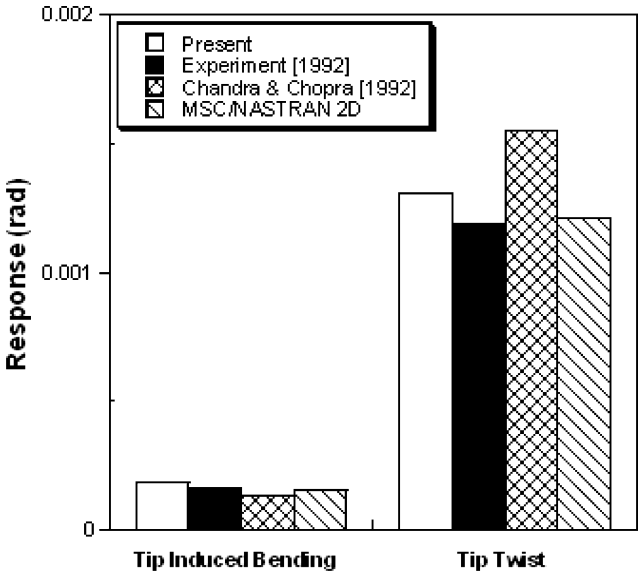

Fig. 13 Comparison of responses for two-cell composite blades (blade 2) under unit tip torque load.

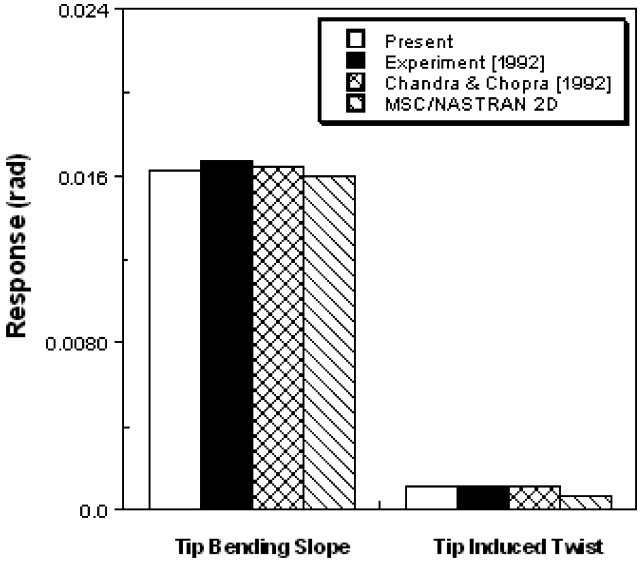

Fig. 14 Comparison of responses for two-cell composite blades (blade 3) under unit tip bending load.

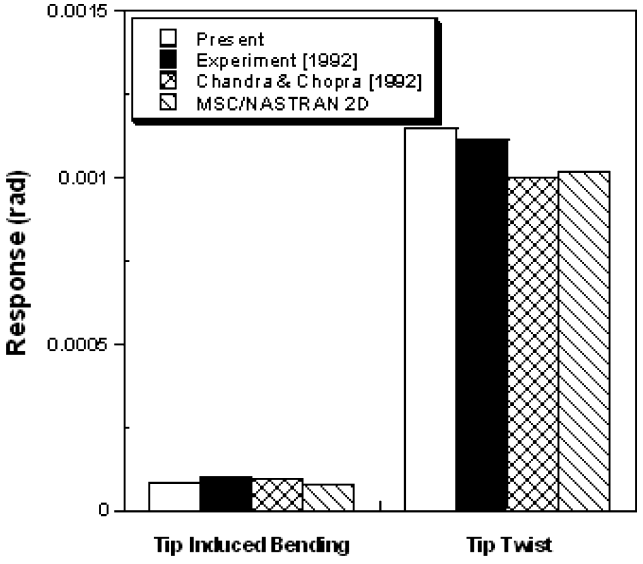

Fig. 15 Comparison of responses for two-cell composite blades (blade 3) under unit tip torque load.

analysis, the present results are within 2.6% of error for the direct tip bending response.

Figure 11 shows the tip twist angles and induced bending slopes of the blade 1 case under a unit tip torque load. A good correlation with experimental results is obtained by the present theory. For this case, the error is 5.9% for the direct tip twist response and 2.2% for the induced bending slopes, respectively. The correlation of the present theory with the NASTRAN analysis is 4.9% for this box 1 case.

Figures 12 and 13 show the structural responses of the 30-deg blade (blade 2) under unit tip bending and torque loads, respectively. It may be seen that the present predictions are in good agreement with the experimental results. The error is less than 10% based on the test results. Note that the results obtained by the present method present better correlations with the experimental results than those obtained by Chandra and Chopra.[4,5] Figures 14 and 15 show the results of blade 3, which has a ply angle of 45 deg. Very good correlation with the experimental test data is clearly seen in these results. For this blade (blade 3), the predicted responses are within 4% of the experimental results.

Conclusions

In the present work, a closed-form formulation for coupled composite blades with multiple-cell sections was developed by use of a mixed approach. The analysis model included the effects of elastic couplings, shell wall thickness, transverse shear deformation, torsion warping, and constrained warping. The beam force–displacement relations of the blade were obtained by using Reissner's semicomplementary energy functional. The resulting (7×7) stiffness matrix idealized the blade at a Timoshenko level of approximation for bending and shear and Vlasov for torsion. The influences of the shell bending strain measures, as well as the membrane strain measures, were incorporated in the formulation. No peculiar assumptions or asymptotic arguments were employed in describing the beam theory. The theory has been correlated with experimental test data, other analysis results found in the literature, and two-dimensional finite element analysis results using MSC/NASTRAN for coupled composite beams and blades with two-cell box sections and two-cell airfoils. Good correlation of results with other methods was obtained for all of the cases considered in this study. The error was generally less than 2% for two-celled composite box beams and 10% for bending–torsion coupled

blades, respectively. It was demonstrated that the errors induced by neglecting the bending strain measures were dependent largely on the geometries and material distributions of the blade. The maximum error encountered was 43.2% for the specific layup where the extension–twisting and bending–shearing couplings (B_{16} and B_{26}) have nonzero values. It was demonstrated also for accurate results that the direction of the integration should be taken with care. The error induced by the inconsistent direction of integration was 29.5% for two-celled composite box beams with extension–bending–torsion couplings.

Acknowledgments

This research was performed for the Smart UAV Development program, one of the 21st Century Frontier Research and Development programs, funded by the Ministry of Science and Technology in the Republic of Korea. The authors acknowledge V. T. Nagaraj from the Alfred Gessow Rotorcraft Center at the University of Maryland, College Park, Maryland, for his helpful comments made during this research.

References

[1]Hodges, D. H., "Review of Composite Rotor Blade Modeling," *AIAA Journal*, Vol. 28, No. 3, 1990, pp. 561–565.

[2]Jung, S. N., Nagaraj, V. T., and Chopra, I., "Assessment of Composite Rotor Blade Modeling Techniques," *Journal of the American Helicopter Society*, Vol. 44, No. 3, 1999, pp. 188–205.

[3]Mansfield, E. H., "The Stiffness of a Two-Cell Anisotropic Tube," *Aeronautical Quarterly*, Nov. 1981, pp. 338–353.

[4]Chandra, R., and Chopra, I., "Structural Behavior of Two-Cell Composite Rotor Blades with Elastic Couplings," *AIAA Journal*, Vol. 30, No. 12, 1992, pp. 2914–2921.

[5]Chandra, R., and Chopra, I., "Coupled Composite Rotor Blades under Bending and Torsional Loads," AHS Specialists' Meeting on Rotorcraft Structures, Williamsburg, VA, Oct. 1991.

[6]Smith, E. C., and Chopra, I., "Formulation and Evaluation of an Analytical Model for Composite Box-Beams," *Journal of the American Helicopter Society*, Vol. 36, No. 3, 1991, pp. 23–35.

[7]Volovoi, V. V., and Hodges, D. H., "Single- and Multicelled Composite Thin-Walled Beams," *AIAA Journal*, Vol. 40, No. 5, 2002, pp. 960–965.

[8]Jung, S. N., Nagaraj, V. T., and Chopra, I., "Refined Structural Model for Thin- and Thick-Walled Composite Rotor Blades," *AIAA Journal*, Vol. 40, No. 1, 2002, pp. 105–116.

[9]Jones, R. M., *Mechanics of Composite Materials*, McGraw–Hill, New York, 1975, Chap. 4.

[10]Gjelsvik, A., *The Theory of Thin Walled Bars*, Wiley, New York, 1981, Chap. 1.

A. Palazotto
Associate Editor